Microrheology of Entangled F-Actin Solutions

M. L. Gardel,[1] M. T. Valentine,[1] J. C. Crocker,[2] A. R. Bausch,[3] and D. A. Weitz[1]

[1]*Department of Physics & DEAS, Harvard University, Cambridge, Massachusetts 02138, USA*

[2]*Department of Chemical and Biomolecular Engineering, University of Pennsylvania, Philadelphia, Pennsylvania 19104, USA*

[3]*Lehrstuhl für Biophysik–E22, Technische Universität München, Garching, Germany*

(Received 28 March 2003; published 7 October 2003)

We measure the viscoelasticity of entangled F-actin over length scales between 1 and 100 μm using one- and two-particle microrheology, and directly identify two distinct microscopic contributions to the elasticity. Filament entanglements lead to a frequency-independent elastic modulus over an extended frequency range of 0.01–30 rad/sec; this is probed with one-particle microrheology. Longitudinal fluctuations of the filaments increase the elastic modulus between 0.1 and 30 rad/sec at length scales up to the filament persistence length; this is probed by two-particle microrheology.

DOI: 10.1103/PhysRevLett.91.158302 PACS numbers: 83.10.Mj, 83.80.Lz, 87.15.La, 87.16.Ka

Filamentous actin (F-actin) is a semiflexible polymer and an essential building block in the cytoskeletal networks that determine cellular mechanics and function [1,2]. *In vitro*, globular actin (G-actin) polymerizes in the presence of K^+ or Mg^{2+} to form polymers whose lengths are polydisperse and of order 10 to 20 μm. These filaments have a persistence length of $l_p \sim 15$ μm, 3 orders of magnitude larger than their diameter, $d \sim 7$ nm [3,4]. Thus, solutions of entangled F-actin are ideal for the study of the dynamics of semiflexible polymer networks. The rheology of semiflexible polymer networks has important contributions from numerous different characteristic length scales and concomitant frequency scales, and is qualitatively different than that of flexible-polymer networks [5–14]. The large persistence length leads to important dynamics of individual filaments that profoundly affect the viscoelasticity of the network. For example, semiflexible polymers become entangled at extremely low volume fractions to form networks with a significant elastic modulus and long viscous relaxation time in comparison to flexible polymers at the same volume fractions. These networks are characterized by an average mesh size, $\xi = 0.3/\sqrt{c_A}$, where c_A is the actin concentration in mg/ml and ξ is measured in μm [15]. However, for semiflexible networks, individual filaments are sterically hindered due to the presence of other filaments at the entanglement length, $l_e \sim \xi^{4/5} l_p^{1/5}$, rather than the mesh size, as is the case for flexible polymers [6,16]. These steric entanglements should result in an elastic modulus that remains constant over an extended range of frequencies. The lower bound in frequency is set by the reptation time, $\tau_r \sim 10^4$ sec, the time it takes a filament to diffusely relax laterally along its tube formed by neighboring filament entanglements. The upper bound is set by the entanglement time, $\tau_e \sim 0.1$ sec, resulting from transverse fluctuations at the largest possible length scale, l_e. However, bulk rheological measurements of F-actin networks do not exhibit this extended plateau [8,13], but instead $G'(\omega)$ increases monotonically with ω at frequencies above ~0.1 rad/sec, and only asymptotically approaches a plateau at even lower frequencies. The excess elasticity is believed to arise from longitudinal fluctuations of the filaments which are coherent over their persistence lengths; such relaxations are unique to semiflexible polymers [5,6]. Thus, the microscopic origins of the rheology canbe ascertained only by determining both the frequency and length scale dependencies.

Microrheological techniques have the potential of probing the response at length scales that are important for actin networks [9–14]. Significant discrepancies are observed between microrheological and bulk measurements of the viscoelasticity of actin networks [13]. However, to date, there have been no attempts to exploit microrheology to elucidate the microscopic origins of the rheology at different length scales and to resolve these discrepancies.

In this Letter, we use one-particle (1P) and two-particle (2P) microrheology to probe the length scale dependence of the rheology and determine the contributions of both the longitudinal fluctuations of the filaments and entanglements to the bulk viscoelasticity of F-actin networks between 0.01–30 rad/sec. We use 2P microrheology to probe the contributions of large length scale fluctuations and 1P microrheology to isolate the contributions of fluctuations at short length scales. We show that the elasticity approaches a frequency-independent plateau when the longitudinal fluctuations have diffusively decayed at the length scale of our probe; by contrast, this time scale is determined by diffusive decay over l_p for bulk measurements. However, the magnitude of this plateau is independent of length scale, allowing both 1P and 2P microrheology to be used to probe the concentration dependent plateau elasticity of F-actin networks.

G-actin solutions are prepared by dissolving lyophilized G-actin in deionized water and dialyzing against fresh G-buffer (2 mM Tris HCl, 0.2 mM ATP, 0.2 mM $CaCl_2$, 0.2 mM DTT, 0.005% NaN_3, *p*H 8.0) at 4 °C for 24 h. Solutions of G-actin are kept at 4 °C and used within 7 days of preparation. Carboxylate modified colloidal spheres (Molecular Probes) [14] are mixed with G-actin

to a volume fraction of ~0.4%. Actin polymerization is initiated by adding 1/10 of the final sample volume of 10× F-buffer (20 mM Tris HCl, 20 mM $MgCl_2$, 1 M KCl, 2 mM DTT, 2mM $CaCl_2$, 5 mM ATP, pH 7.5) and mixing gently for 10 sec. The sample is loaded into a 5 mm × 10 mm × 1 mm glass sample chamber, sealed with high-vacuum grease and equilibrated for 1 h at about 25 °C. We image approximately 100 spheres with an inverted microscope in bright field (40 ×; N.A. = 0.85, air) and record their dynamics at 30 frames/sec using a CCD camera with a shutter speed of 0.5 msec [17]. Several thousand frames are captured, ensuring good statistical accuracy for time scales up to 100 times the frame rate. Particle centers are detected in each frame to an accuracy of 20 nm and the time evolution of the position of each particle is determined [18]. To avoid wall effects, we image 100 μm into the sample.

We calculate the one-dimensional ensemble averaged mean-squared displacement $\langle \Delta x^2(\tau) \rangle$ (1P MSD) and scale the results by the particle radius, a, to reflect the size-dependent viscous drag. In a solution of 0.9 mg/ml F-actin, where $\xi = 0.3$ μm, the scaled MSD of particles with $a = 0.42$ μm ($a/\xi \approx 1.5$) exhibits very little time evolution, reaching a constant value for $\tau > 0.1$ sec, as shown by the solid circles in Fig. 1. The magnitude and frequency dependence of the MSD remain unchanged for smaller particles with $a = 0.32$ μm ($a/\xi \approx 1$), as shown by the solid triangles in Fig. 1. By contrast, the scaled MSD of even smaller particles, with $a = 0.23$ μm ($a/\xi \approx 0.6$) is dramatically different, evolving as $\tau^{\sim 0.4}$, as shown by the solid squares in Fig. 1. By examining individual particle trajectories, we find that all the 0.32-μm and 0.42-μm particles remain caged, whereas some of the 0.23-μm particles can permeate through the network [19]. Since the 1P MSD probes the local microenvironment at length scales of ~a, small changes in particle size have dramatic effects on the 1P MSDs.

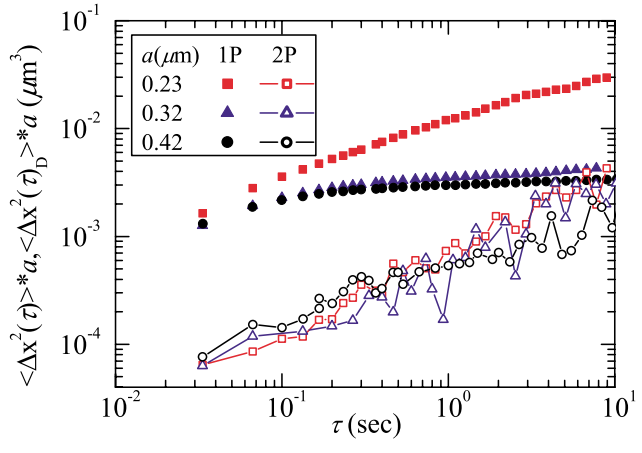

FIG. 1 (color online). Comparison of 1P (symbols) and 2P (open symbols with lines) MSDs in 0.9 mg/ml F-actin ($\xi = 0.3$ μm).

To examine dynamics at length scales much larger than a, we determine the correlated displacements of pairs of particles, i and j, separated by a distance, 10 μm $< R^{ij} <$ 100 μm. We average over time, t, and over all distinct pairs of particles ($i \neq j$) to calculate the two-particle displacement correlation tensor,

$$D_{\alpha\beta}(r,\tau) = \langle \Delta r^i_\alpha(t,\tau) \Delta r^i_\beta(t,\tau) \delta[r - R^{ij}(t)] \rangle_{i \neq j,t}, \quad (1)$$

where Δr^i_α is the displacement of the ith particle in α component of the direction. At length scales, r, where the material behaves as a bulk viscoelastic material, the correlated motion will decay as $1/r$ [17,20,21]. From the R^{ij} where we observe a $1/r$ decay, we extrapolate the correlated motion to a, and define the two-particle mean-squared displacement, $\langle \Delta r^2(\tau) \rangle_D = 2r/aD_{rr}(r,\tau)$ (2P MSD). Physically, the 2P MSD reflects the one-particle motion expected from long-wavelength modes in the material; thus, by examining correlations up to 100 μm, we are able to use 0.5-μm particles to measure mechanical response in entangled F-actin at length scales up to an order of magnitude longer than individual filaments. The scaling factor of $2/a$ is obtained by assuming the surrounding medium is incompressible, thus having a Poisson ratio of $\sigma = 1/2$ [20]. We can directly test this assumption by comparing the transverse, $D_{\theta\theta}$ and $D_{\phi\phi}$, to the longitudinal, D_{rr}, components of the two-particle correlation tensor from Eq. (1), and calculating

$$\frac{D_{\theta\theta}}{D_{rr}} = \frac{D_{\phi\phi}}{D_{rr}} = \frac{3 - 4\sigma}{4(1 - \sigma)}. \quad (2)$$

This ratio results from calculating the strain field of a point stress in an elastic medium [17,20,21]. We find that F-actin is incompressible for $0.03 < \omega < 30$ rad/sec and $\sigma = 1/2$ as shown in Fig. 2.

The frequency dependence and magnitude of the 2P MSD of 0.42-μm spheres in 0.9 mg/ml actin is qualitatively different than the 1P MSD. At $\tau = 0.1$ sec, the 2P MSD is an order of magnitude smaller than the 1P MSD; moreover, it scales as $\tau^{0.5}$ whereas the 1P MSD is essentially constant in time, as shown in Fig. 2. However, at

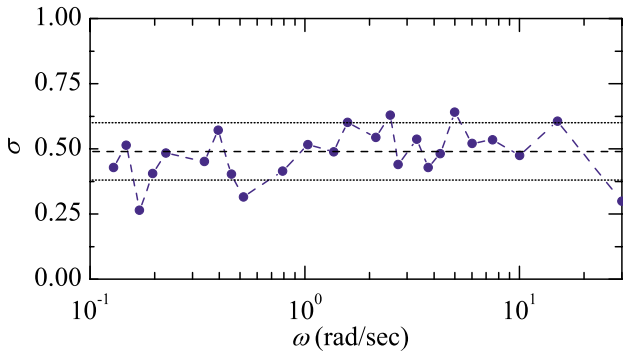

FIG. 2 (color online). The Poisson ratio of 0.9 mg/ml F-actin probed with 0.32-μm particles.

$\tau = 10$ sec, the 1P and 2P MSDs converge to similar values. Similar behavior is observed with the 0.32-μm spheres. Remarkably, the 2P MSD of the 0.23-μm particles also overlays well with the 2P MSDs obtained with the larger probes. Although the 0.23-μm spheres can permeate through the network, these motions are not correlated at long distances; the two-particle analysis reflects only that portion of the tracer motion due to advection by strain fluctuations of the network.

We measure the 2P MSD of 0.42-μm particles in a 1 mg/ml F-actin solution and use the generalized Stokes-Einstein relation [22] to obtain a good approximation of the frequency-dependent bulk elastic modulus, $G'(\omega)$, and viscous modulus, $G"(\omega)$ as shown by the closed and open circles, respectively, in Fig. 3(a). These are in excellent accord with the bulk values, shown by the closed and open triangles, obtained using a home-built stress-controlled rheometer with a parallel plate geometry [8,13]; bulk properties are also correctly measured with the 2P MSDs of the 0.32 and 0.23-μm particles. In 1 mg/ml F-actin, between 0.1 and 30 rad/ sec, 2P microrheology measures a viscoelastic response with the elastic and loss moduli similar in magnitude, and proportional to 0.5 as shown by the solid line in Fig. 3(a). At the lowest frequencies, below 0.1 rad/ sec, the elastic modulus begins to dominate and we infer a plateau modulus, $G_o \approx$ 0.2 Pa. Similarly, we find the 2P MSD of 0.5-μm particles yields results in good accord with bulk measurements of the frequency-dependent viscoelasticity for a 0.3 mg/ml F-actin solution, as shown in Fig. 3(b), and

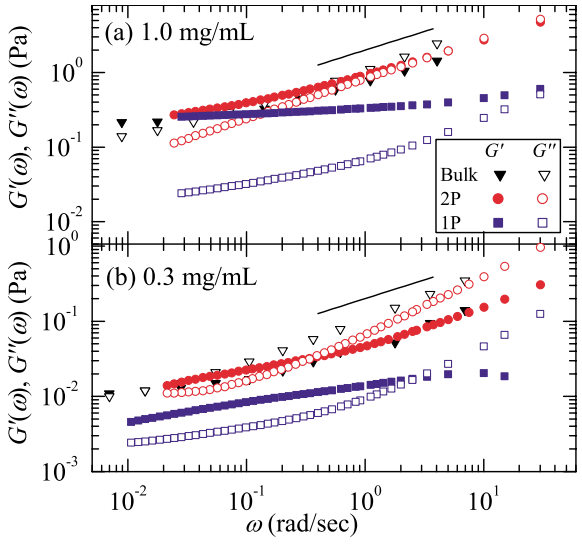

FIG. 3 (color online). Comparison between the elastic modulus, $G'(\omega)$ (closed symbols), and loss modulus, $G''(\omega)$ (open symbols) obtained from 1P (squares) and 2P (circles) microrheology and from a conventional rheometer (triangles) for (a) 1.0 mg/ml F-actin probed with 0.42-μm beads and (b) 0.3 mg/ml F-actin with 0.5-μm beads. The solid line in both (a) and (b) shows $\omega^{0.5}$.

we infer $G_o \approx 0.01$ Pa. While the magnitudes and frequency dependence of 2P moduli are robust, crossover frequencies cannot be precisely determined as they are very sensitive to variations in the smoothing of the 2P MSD required to determine the viscoelastic moduli [22]. Thus, examining the pairwise correlated motion of micron-sized particles separated between 10 and 100 μm successfully probes the properties observed at macroscopic length scales with traditional rheology.

To elucidate the microscopic origins of this viscoelasticity, we use the 1P MSD, interpreted with the generalized Stokes-Einstein relation, to examine length scale dependence of the viscoelastic response. For 1 mg/ml F-actin, the 1P microrheology using 0.42-μm particles ($a/\xi \approx 1.5$) exhibits a well-defined plateau over the extended frequency range of 0.03 to 30 rad/ sec, as shown in Fig. 3(a) by the solid and open squares. By contrast, the dynamics of 0.5-μm particles in 0.3 mg/ml F-actin yield 1P microrheology results that significantly underestimate the bulk viscoelasticity, by nearly an order of magnitude over the entire frequency range, as shown in Fig. 3(b). In this case, $a/\xi \approx 0.6$, and particle motion is again dominated by permeation through the network; any similarity in the frequency dependence between the microrheology and the bulk measurements is a pure coincidence [19]. We find that when $a/\xi \geq 1$, 1P microrheology measures a frequency-independent elastic modulus between 0.01 and 30 rad/ sec consistent with the plateau modulus observed in a 2P or bulk measurement of entangled actin at frequencies below 0.1 rad/ sec.

The observed independence of the 1P viscoelasticity in both frequency and particle size, and its convergence with the two-particle results at the lowest frequency strongly suggest that the discrepancies between 1P and 2P microrheology for particle sizes $a \geq \xi$ arise from the nature of the coupling between the particles and the excitations responsible for the elasticity of the network [23]. At intermediate frequencies, between 0.1 and 30 rad/ sec, longitudinal density fluctuations of the filaments significantly contribute to the bulk rheological response; these relax by diffusing along the filament [5,6]. Thus, the lowest frequency of these excitations that affects both 2P microrheology and bulk rheology is determined by the time taken for the density fluctuation to diffuse a persistence length, $\tau_l \sim \tau_e(l_p/l_e) \sim 10$ sec, where $\tau_e \sim \zeta l_e^4/l_p k_B T \sim 0.1$ sec and where ζ is the effective friction coefficient of the filament in solution, k_B is Boltzmann's constant, and T is the temperature. However, 1P motion will sense only fluctuations on length scales of a, and these relax much more quickly, on time scales of $\tau_l' \sim \tau_e(a/\sqrt{l_e l_p})^2 \sim 0.1$ sec; thus 1P microrheology will not probe elasticity due to the longitudinal fluctuations for $\omega < \omega_l \sim (\tau_l')^{-1}$ [23]. By contrast, because of its larger effective length scale, 2P microrheology samples these excitations in the same fashion as bulk measurements, and thus yields the bulk response in the frequency regime

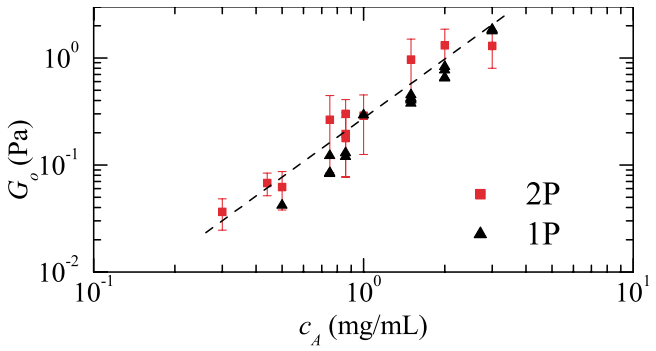

FIG. 4 (color online). The concentration dependence of the elastic modulus at 0.05 rad/sec, G_o, obtained from 1P (triangles) and 2P (squares) microrheology. The two techniques are similar in magnitude and both scale as $G_o \sim c_A^{1.8\pm0.4}$. The dashed line shows a scaling of $c_A^{1.8}$.

0.1–10 rad/sec. Interestingly, 1P microrheology begins to exhibit additional relaxations at frequencies comparable to τ_l^{-1}, where longitudinal excitations on the scale of a begin to contribute.

The other significant contribution to the bulk viscoelasticity below 30 rad/sec is the elasticity due to entanglements of the filaments that occur at a scale $l_e \sim 0.65$ μm for a 1 mg/ml F-actin network. It is these collisions that determine the plateau elasticity $G_o \sim \rho k_B T/l_e$ where ρ is the density of filaments. By recognizing that $\rho \sim c_A$ and recalling that $c_A \sim 1/\xi^2$, we obtain $G_o \sim c_A^{7/5}/l_p^{1/5}$. Because this plateau modulus arises from a length scale, $l_e \sim a$, it is exactly this frequency-independent plateau modulus that 1P microrheology measures at all frequencies in our experiment. Thus, 1P microrheology exhibits the same concentration dependence of G_o as does 2P microrheology; we find $G_o \sim c_A^x$, where $x = 1.8 \pm 0.4$, as shown in Fig. 4. This is in good agreement with the behavior seen experimentally [8,12] and with theoretical predictions [8,24]. The error bars plotted for the moduli measured with 2P microrheology reflect the statistical uncertainty of G_o for each measurement; this is substantially more than the statistical uncertainty in the 1P measurements, but is comparable to the sample-to-sample variation. The agreement between the plateau modulus obtained from 1P and 2P microrheology as a function of c_A at long times clearly suggests that local heterogeneities, such as those due to depletion or preferential binding to the bead, have little or no influence on the microrheology measurements. Thus, both 1P and 2P microrheology measure the low frequency plateau of the elastic modulus due to filament entanglements.

A single multiparticle tracking experiment requiring only 30 μl of sample volume and thermal energy provides a wealth of information. The addition of crosslinking proteins will disrupt the longitudinal fluctuations of the filaments, reducing their importance. This augurs well for the application of 1P microrheology to *in vitro* networks that more closely mimic the cytoskeleton through the addition of crosslinking proteins. Moreover, it also suggests that 1P microrheology may also be adequate for *in vivo* measurements of cells.

We thank Tony Maggs and Fred MacKintosh for valuable discussions and A. Popp and B. Hinner for bulk rheology data. This work was supported by the NSF (No. DMR-9971432 and No. DMR-0243715). A. B. acknowledges support from the Emmy Noether Program of the DFG. M. L. G. was supported by Lucent GRPW.

[1] B. Alberts, D. Bray, A. Johnson, J. Lewis, M. Raff, K. Roberts, and P. Walter, *Essential Cell Biology* (Garland, New York, 1989).
[2] T. Pollard and J. Cooper, Annu. Rev. Biochem. **55**, 987 (1986).
[3] A. Ott, M. Magnasco, A. Simon, and A. Libchaber, Phys. Rev. E **48**, R1642 (1993).
[4] F. Gittes, B. Mickey, J. Nettleton, and J. Howard, J. Cell Biol. **120**, 923 (1993).
[5] A. Maggs, Phys. Rev. E **55**, 7396 (1997).
[6] D. C. Morse, Macromolecules **31**, 7044 (1998).
[7] F. Gittes and F. MacKintosh, Phys. Rev. E **58**, R1241 (1998).
[8] B. Hinner, M. Tempel, E. Sackmann, K. Kroy, and E. Frey, Phys. Rev. Lett. **81**, 2614 (1998).
[9] F. Amblard, A. Maggs, B. Yurke, A. N. Pargellis, and S. Leibler, Phys. Rev. Lett. **77**, 4470 (1996).
[10] B. Schnurr, F. Gittes, F. C. MacKintosh, and C. F. Schmidt, Macromolecules **30**, 7781 (1997).
[11] T. Gisler and D. A. Weitz, Phys. Rev. Lett. **82**, 1606 (1999).
[12] A. Palmer, T. G. Mason, J. Y. Xu, S. C. Kuo, and D. Wirtz, Biophys. J. **76**, 1063 (1999).
[13] F. G. Schmidt, B. Hinner, and E. Sackmann, Phys. Rev. E **61**, 5646 (2000).
[14] J. L. McGrath, J. H. Hartwig, and S. C. Kuo, Biophys. J. **79**, 3258 (2000).
[15] C. F. Schmidt, M. Barmann, G. Isenberg, and E. Sackmann, Macromolecules **22**, 3638 (1989).
[16] A. Semenov, J. Chem. Soc. Faraday Trans. 2 **82**, 317 (1986).
[17] J. C. Crocker, M. T. Valentine, E. R. Weeks, T. Gisler, P. D. Kaplan, A. G. Yodh, and D. A. Weitz, Phys. Rev. Lett. **85**, 888 (2000).
[18] J. C. Crocker and D. G. Grier, J. Colloid Interface Sci. **179**, 298 (1996).
[19] I. Wong *et al.* (to be published).
[20] L. Landau and E. Lifshitz, *Theory of Elasticity* (Pergamon Press, Oxford, 1986).
[21] A. J. Levine and T. C. Lubensky, Phys. Rev. Lett. **85**, 1774 (2000).
[22] T. Mason, Rheol. Acta **39**, 371 (2000).
[23] A. Maggs, Phys. Rev. E **57**, 2091 (1998).
[24] D. C. Morse, Phys. Rev. E **63**, 031502 (2001).